SCIENCE CHINA
Information Sciences

• **Supplementary File** •

A High Precision Two-Axis GMR Angular Sensor Manufactured by Post-Annealing

Zitong Zhou[1,2], Zhiqiang Cao[1,3], Shaohua Yan[1,2], Xiaolong Wang[1,2], Libo Xie[1,2], Shiyang Lu[1,2], Dapeng Zhu[1,2*], Qunwen Leng[1*] & Weisheng Zhao[1*]

[1]*School of Integrated Circuit Science and Engineering, Beihang University, Beijing* 100191, *China;*
[2]*Beihang Qingdao Microelectronics Research Institute, Beihang University, Qingdao* 266000, *China;*
[3]*National Key Lab of Spintronics, Institute of International Innovation, Beihang University, Yuhang District, Hangzhou,* 311115, *China*

Appendix A Film Stack Structure and Characterization

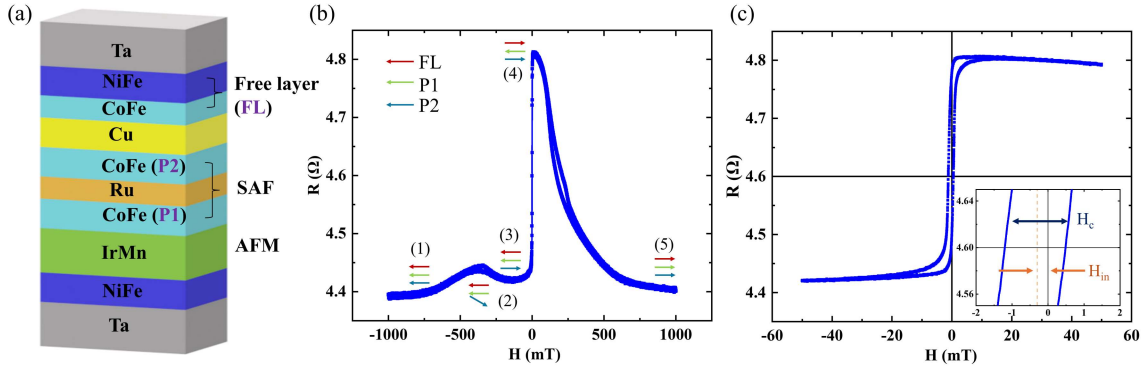

Figure A1 (a) The structure of GMR film stack deposited on the Si wafer with the SAF layer (CoFe/Ru/CoFe).(b) The hysteresis loops of the GMR stack under 1 T with the indicated magnetic directions of two pinned layers (P1, P2) and free layer (FL), respectively. (b) The R-H curve under 50 mT field.

Figure. A1(a) shows the GMR layer stacks with a structure of Ta(5.0)/$Ni_{81}Fe_{19}$(2.0)/$Ir_{20}Mn_{80}$(7.5)/$Co_{70}Fe_{30}$(2.0)/Ru(0.85)/$Co_{70}Fe_{30}$(2.1)/Cu(1.9)/$Co_{70}Fe_{30}$(1.0)/$Ni_{81}Fe_{19}$(2.0)/Ta(3.0) (thickness in nm). The hysteresis loop of the stack is shown in Fig. A1(b). We sweep the field $\pm$ 1 T to make the antiferromagnetic (AFM) layer reversed. The $Co_{70}Fe_{30}$/Ru/$Co_{70}Fe_{30}$ constitutes a synthetic antiferromagnetic (SAF) layer. Due to the exchange coupling, the magnetization directions of the upper and lower ferromagnetic layers in the SAF structure are kept antiparallel when the external field is small. We define the upper ferromagnetic layer as the P1 and the lower ferromagnetic layer as the P2. When the external magnetic field is large enough to overcome the exchange bias of the AFM layer and the coupling effect in the SAF structure, the magnetization directions of all magnetic layers are consistent with the direction of the external field, such as state 1 and 5. As the external field decreases, the coupling effect in the SAF structure will restore the magnetization directions of the P1 layer and P2 to antiparallel, that is, the change from 1 to 3 state. From state 3 to 4, the inversion of the free layer brings about a huge magnetoresistance (MR) change. As shown in Fig. A1(c), the H_c of the hysteresis loop is around 0.9 mT, and the H_{in} is 0.4 mT, the output in the linear region is symmetrical about the Y=0 axis. And the GMR ratio reaches 8.8%.

Appendix B Effect of secondary annealing field and shape anisotropy on pinning direction

The annealing process is performed after the patterning process. The patterning process of the GMR strips is accomplished by photolithography and ion beam etching. In the first annealing, the large field of 1 T unified the direction of all magnetic moments to be consistent with the direction of the external magnetic field. Then, a reverse weak magnetic field is applied and the SAF structure enters the spin-flip state. The field for the second annealing was set to 80 mT, 95 mT, and 110 mT.

Figure. B1(a) and B1(b) respectively show the $MR\% - H$ curves of the three kinds of GMR transducer designs when the second annealing field is 80 mT. Fig. B1(a) shows the MR% of the 90° GMR stripe reaches 6.35%, and the output behavior of the 45° and 135° stripes is the same when the field is along the x-axis. When the external field is along the y-axis, as shown in Fig. B1(b), the magnetization flip of the 45° stripe is from antiparallel to parallel, and the flip behavior of the 135° stripe is the opposite.

* Corresponding author (email: zhudp@buaa.edu.cn, lengqw@bhqditi.com, weisheng.zhao@buaa.edu.cn)

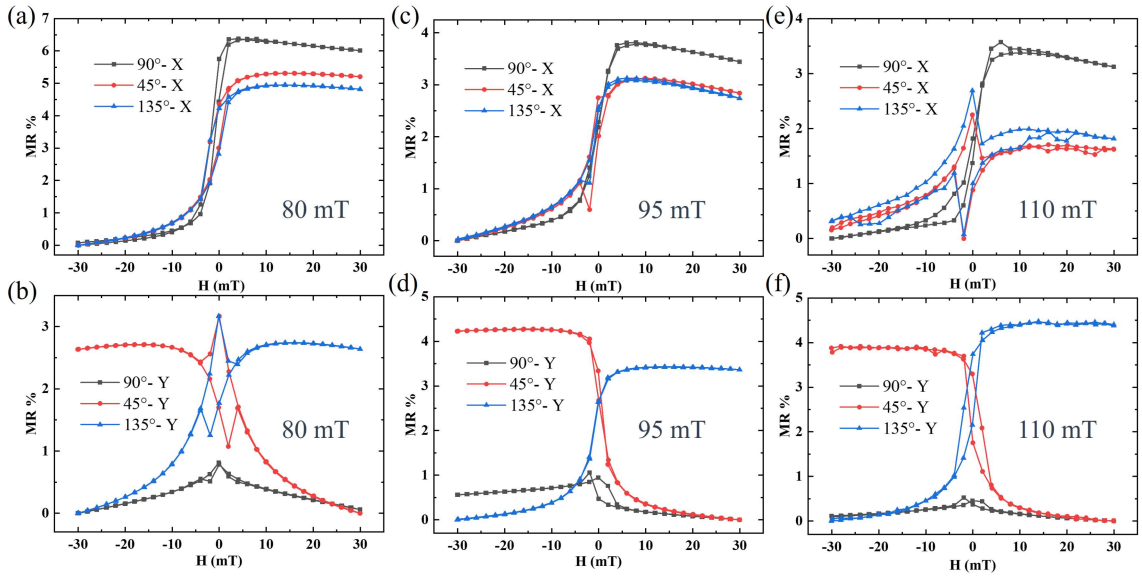

Figure B1 $MR\% - H$ output curves of 45°, 135°, and 90° GMR stripe designs under the second annealing condition of 80 mT in X (a) and Y (b) directions; The $MR\% - H$ output curves in the X (c) and Y(d) direction at 95 mT and the $MR\% - H$ output curves in the X (e) and Y (f) directions at 110 mT.

The H_c reaches 4.5 mT and the MR% of the two kinds of stripe is only 2.7%. When the annealing field increases to 95 mT, the $MR - H_y$ curve for the 90° design transducer, which does not show the symmetrical behavior of the magnetic field sweeping from -30 mT to 30 mT, that is, H_y is not perpendicular to P2. The H_c of the 90° stripe decreases to 0.3 mT and the MR% decreases to 3.8% when the field is along the X-axis. The lowest point of the curve is not at zero field, which means that FL and P1 are not ferromagnetically coupled, and the shape anisotropy affects the direction of FL. The H_c of 45° and 135° stripes decrease to 0.4 mT and 0.1 mT, and the MR% increase to 4.28% and 3.42% when a field is along the Y-axis, as shown in Fig. B1(c) and B1(d). Then the field increases to 110 mT, the hysteresis increases again, the MR% of the 90° stripe decreases to 3.4% in the X-axis field and the MR% of 45° and 135° stripes are 3.9% and 4.5% in the Y-axis field, as shown in Fig. B1(e) and B1(f).

Under the combined effect of shape anisotropy energy and Zeeman energy, the magnetization directions of P1 and P2 will deviate from the initial annealing direction and keep opposite. The orientation is fixed after cooling. For the linearization of sensor output, it is necessary to modulate the easy axis of the free layer to be perpendicular to the external field. The direction of the easy axis is affected by the joint effect of the shape anisotropy energy and the interlayer coupling energy between the P1 layer and the FL. If the interlayer coupling between P1 and the FL is strong, the shape anisotropy is no longer a single factor affecting the easy axis direction of the free layer, so the magnitude of the second annealing field can also affect the easy axis direction. At 95 mT, the easy axis and the external magnetic field are close to 90°, so the H_c is the smallest. At 80 mT and 110 mT, the larger hysteresis means that the easy axis of the free layer deviates from the vertical direction of the external magnetic field, indicating under-regulation and over-regulation.

The pinned directions of the 45° and 135° GMR stripe are closest to —45° and 45°, with opposite MR change trends and the Hc are 0.4 mT and 0.1 mT when the reverse magnetic field is 95 mT. The 90° GMR stripe has a decrease in MR%, from 6.35% to 3.8%, due to the pinned direction offset by 5° from the annealing direction, and the H_c is 0.3 mT. Therefore, the best output of the full-bridge and half-bridge sensors can be obtained.

Appendix C Geomagnetic angle response of two-axis GMR angle sensor.

Figure. C1(a) is the output curve of the two-axis GMR sensor after normalization and a time-varying curve of the sensed geomagnetic field angle, which is obtained by calculating the phase vectors of the two-axis signals. The two-axis curves both show a sinusoidal response. The 90° phase shift between the X-axis and Y-axis signals indicates the orthogonality of the two-axis sensing directions.

To intuitively obtain the quadrature error and signal offset of the x and y signals, draw the X and Y axis signals on the $X - Y$ plane, as shown in Fig. C1(b). After merging, the fitting curve is a circle with a diameter of 1. The quadrature phase error φ of the two-axis output signals can be calculated by the formula [1],

$$M_\theta = \sqrt{(X_\theta)^2 + (Y_\theta)^2}, \tag{C1}$$

$$M_{\pi+\theta} = \sqrt{(X_{\pi+\theta})^2 + (Y_{\pi+\theta})^2}, \tag{C2}$$

$$\varphi = 2 \times \arctan(M_{\pi+\theta} - \frac{M_\theta}{M_{\pi+\theta}} + M_\theta), \tag{C3}$$

Figure. C1(c) shows the data points of the two-axis orthogonal error φ which is calculated by Eq. (3) when the two-axis sensor rotates from 0° to 360° under the geomagnetic field. The φ is between —0.04 - 0.04.

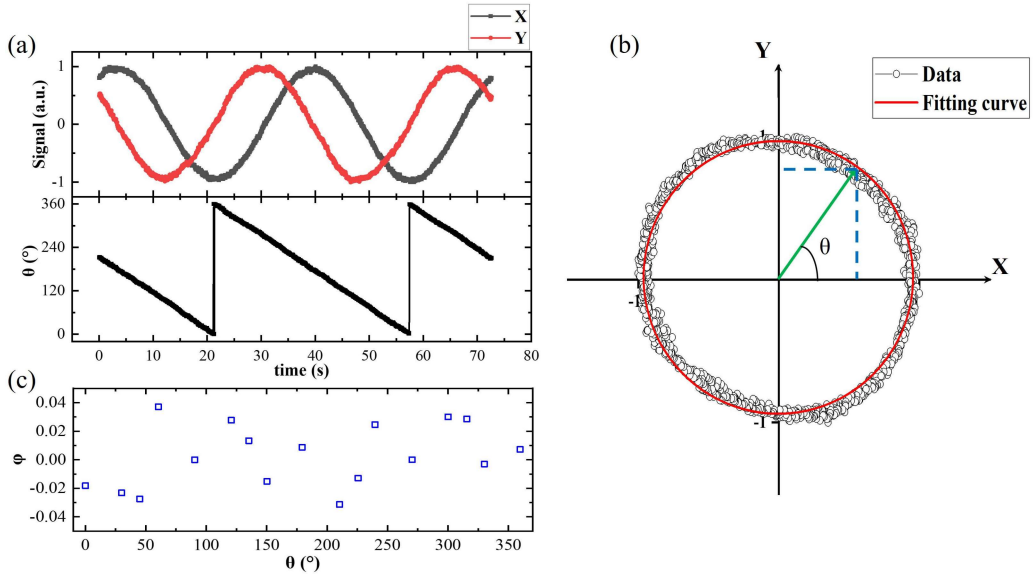

Figure C1 (a) The output curve of the two-axis GMR sensor after normalization and the time-varying curve of the sensed geomagnetic field angle. (b) The change curve of the X signal and Y signal in the $X-Y$ plane. (c) Data points of two-axis orthogonal error φ as the turntable rotates 360°.

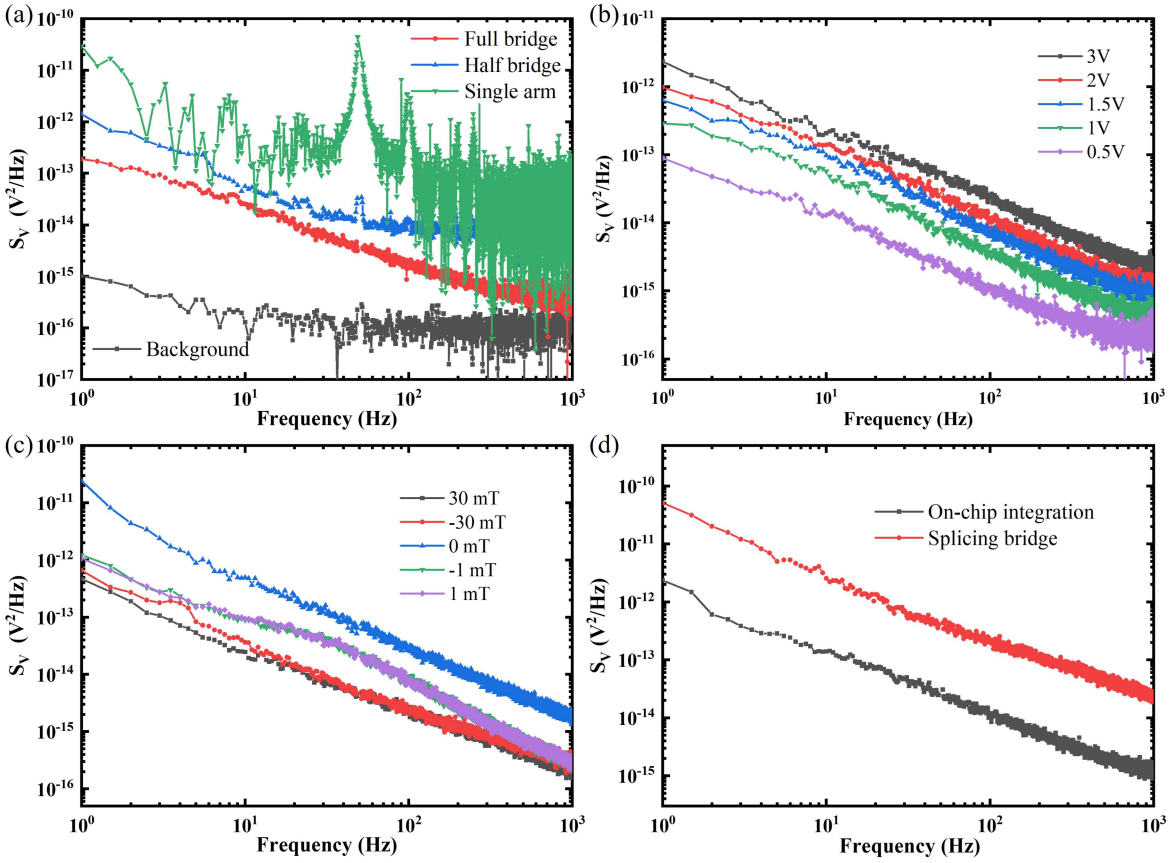

Figure D1 (a) The noise PSD of the full-bridge GMR sensor, half-bridge sensor, and single GMR stripes arm. (b)The noise PSD of the GMR full Wheatstone-bridge sensor under different bias voltages, from 0.5 V to 3 V. (c) The noise PSD of the GMR devices under different external magnetic fields. (d) The noise PSD of the splicing bridge sensor and integrated bridge sensor.

Appendix D Discussion of the noise performance of the GMR sensors

The low-frequency noise of the GMR sensor mainly consists of $1/f$ noise, thermal noise, and random telegraph noise (RTN) [2–4].To discuss the detection limit of the sensor, the noise PSD of GMR sensors with different structures was tested by a self-built noise test system. Fig. D1(a) shows the noise PSD of the three kinds of GMR devices, including full-bridge, half-bridge, and single-bridge arms, applying a voltage of 1.5 V to the sensor of the bridge circuit, and added a DC of 10 uA to the single bridge arm. The background noise PSD of the system is lower than 10^{-16} V^2/Hz. The bridge circuit has lower low-frequency noise than a single GMR transducer. The bridge circuit has lower low-frequency noise than a single transducer. Since the noise PSD curves within 100 Hz with frequency at a ratio of $1/f$, the influence of RTN noise can be ignored. The thermal noise is the main component of white noise in GMR sensors. So the white noise PSD can be expressed as [2],

$$S_V^{thermal} = 4Rk_BT, \tag{D1}$$

where R is the resistance of the tested device, and k_B is the Boltzmann constant. Ideally, the output voltage should be zero when the external magnetic field is zero if the four bridge arm resistances are matched. However, due to manufacturing error and the contact resistance, it is difficult to be the same for the four bridge arm resistances. The output resistance of the half-bridge sensor is larger than that of the full-bridge sensor, so the half-bridge sensor has higher white noise.

Figure. D1(b) illustrates the noise PSD of the GMR full Wheatstone-bridge sensor under different bias voltages, from 0.5 V to 3 V, without an external field. It shows that the $1/f$ noise PSD of the GMR full-bridge sensor increases as the input voltage increases and is proportional to the voltage. Therefore, reducing the driving voltage of the sensor can effectively suppress the $1/f$ noise and improve the detectivity.

Figure. D1(c) is the noise PSD of the GMR devices under different external magnetic fields. It can be seen that under low magnetic fields ($\pm$1 mT), there is an obvious line pattern of Magnetic Barkhausen noise, which is a kind of noise caused by the reciprocating motion of the magnetic domain wall. When the external magnetic field further increases, $1/f$ noise begins to dominate again. Therefore, applying a certain bias magnetic field to stabilize the magnetization state of the free layer can effectively suppress the magnetic noise in the GMR devices and improve the signal-to-noise ratio of the sensor. The noise PSD of the splicing bridge sensor and integrated bridge sensor was compared in Fig. D1(d). The noise PSD of the on-chip integrated sensor is an order of magnitude lower than that of the spliced sensor.

References

1 Reig, C.; Cardoso, S.; Mukhopadhyay, S. C., Gmr Based Sensors for Ic Current Monitoring. In Giant Magnetoresistance (GMR) Sensors, Springer: London, 2013; Vol. 6, pp 109-111.

2 Lei, Z. Q.; Li, G. J.; Egelhoff, W. F.; Lai, P. T.; Pong, P. W. T., Review of Noise Sources in Magnetic Tunnel Junction Sensors. IEEE Transactions on Magnetics 2011, 47, 602-612.

3 Hu, J.; Pan, M.; Tian, W.; Chen, D.; Zhao, J.; Luo, F., 1/F Noise Suppression of Giant Magnetoresistive Sensors with Vertical Motion Flux Modulation. Applied Physics Letters 2012, 100, 244102.

4 Nagumo, T.; Takeuchi, K.; Yokogawa, S.; Imai, K.; Hayashi, Y. In New Analysis Methods for Comprehensive Understanding of Random Telegraph Noise, 2009 IEEE International Electron Devices Meeting (IEDM), 7-9 Dec. 2009; 2009; pp 1-4.